A Direct Ion Imaging Approach for Investigation of Ion Dynamics in Multipole Ion Guides

Sarfaraz U. A. H. Syed[a,b], Simon Maher[c], Gert B. Eijkel[a], Shane R. Ellis[a,d], Fred Jjunju[c], Stephen Taylor[c] and Ron M. A. Heeren[a,b,d]

[a]FOM Institute AMOLF, Science Park 104, 1098 XG Amsterdam, The Netherlands

[b]TI-COAST, Science Park 904, 1098 XH Amsterdam, The Netherlands

[c]Department of Electrical Engineering and Electronics, University of Liverpool, Liverpool, L69 3GJ, UK

[d] M4I, The Maastricht MultiModal Molecular Imaging Institute, University of Maastricht, Universiteitssingel 50, 6229 ER Maastricht, The Netherlands

Address reprint requests to:

Prof. Dr. Ron. M. A. Heeren

M4I, Maastricht University

Universiteitssingel 50

6229 ER Maastricht

The Netherlands

Abstract

A key requirement of electrospray ionization (ESI) and other techniques facilitating ionization at elevated pressures is the efficient transport of free gas-phase ions into the high vacuum region of the mass spectrometer. Radio frequency (RF) multipole ion guides that allow for collisional cooling are one of the most popular means of achieving this. However, their performance is highly dependent on several experimental factors including pressure and various electrode potentials along the ion path. To experimentally visualise these effects we have employed a position sensitive detector at the exit of a quadrupole mass spectrometer (QMS) instrument operated in RF only mode that employs an RF only octopole as a collisional cooling ion guide. This allows the spatial distribution of the ions, and its dependence on experimentally determined conditions, to be directly visualised at the exit of the quadrupole. This investigation provides a detailed insight into the ion dynamics occurring inside multipole ion guides. This knowledge can directly be applied to instrument development and to improve the ion transmission efficiency, and thus sensitivity. Numerical simulations using custom developed trajectory simulation software are compared and contrasted with the experimental observations.

Graphical Abstract

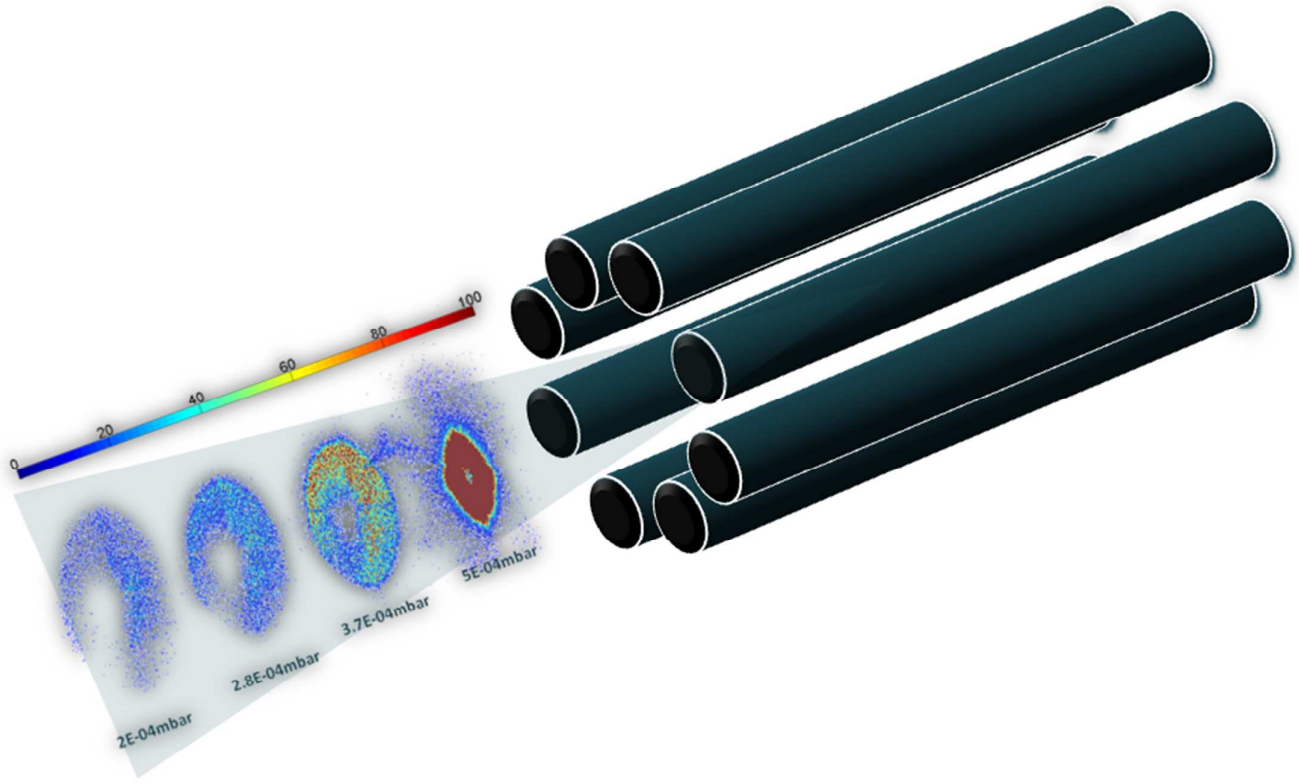

Collisional Focussing

Introduction

Octopoles and/or quadrupoles [1] are the most widely used collisional cooling multipole ion guides employed to couple ambient ionization sources to various mass analyzers. In cooling ion guides, ion collisions with buffer gas molecules take place. The collisions with the background gas dampens the ion trajectories towards the centre of the ion guide thus improving ion focusing for the ions entering the mass analyzer section of an instrument. Another, rapidly developing application of the collisional cooling RF multipoles is for accumulation of ions, e.g., in linear quadrupole ion traps mass spectrometers [2].

Ion dynamics inside ion guides when employed for collisional cooling are different when compared to ion guide operation under ultra high vacuum conditions. The ion-neutral collisions and ion-ion interactions in the cooling ion guides will change the nature of ion behaviour during transport. Collisional cooling effects have been investigated previously. Original works on collisional damping or collisional focusing of ion trajectories in three-dimensional ion traps were published in 1970s [3-5]. In the case of 2D RF multipoles, collisional focusing effects were first reported by Douglas and French in 1992 [6]. Hang and Lewis investigated the practical considerations when using RF only quadrupole ion guide for atmospheric pressure ionization sources with time-of-flight mass spectrometry [7]. In concurrance with [6], they found improved transmission at higher gas pressures inside the collisional ion guide. Chernushevich and Thomson improved collisional cooling for large compact ions by trapping ions with increased cooling times in addition to a higher pressure operation of the ion guides [8]. Few investigations in literature report ion density distributions inside cooling multipoles. Theoretical treatments of the radial ion density distribution in the collisional RF multipoles have been reported in [9-11] by taking into account the rapidly changing RF field, ion–neutral collisions and ion–ion (space charge) interactions. It was

mentioned that under heavy ion loading conditions the ions will have a radial distribution with a radius increasing with *m/z*. The phenomenon observed in [10, 11] was confirmed experimentally for collisional RF quadrupoles that are used both for the external accumulation and as ion guides [12]. More recently, in our previous work [13] using the position sensitive Timepix detector we have experimentally observed radial distribution of different m/z ions exiting a linear quadrupole mass spectrometer. The findings were in agreement to the work reported in [12], and it was concluded in [13] that the observed radial distribution reflects the entrance conditions of ions imparted via a collisional cooling octopole into quadrupole mass filter (QMF).

In this paper, we have used the Timepix detector to visualize for the very first time experimentally how the different source conditions affect the spatial distribution of ions through an ion guide. It is demonstrated how the collisional focusing inside a RF octopole ion guide brings ions closer to the ion guide axis at higher gas pressures. Moreover, the properties of the ion beam exiting an octopole ion guide-quadrupole mass spectrometer instrument are studied for different operating conditions.

Methods

Experimental

Measurements were performed using the instrument described in [13, 14]. The description of the system is reproduced here for completeness. Figure 1 shows a 2D schematic diagram with visualization of different potentials used in the system. The MCP/Timepix detector [15, 16], mounted on a vacuum flange, is placed inside the vacuum chamber 8 cm from the exit side of the QMF (Quadrupole ABB Extrel, from Extrel, Pittsburgh, USA). Ions are created by electrospray ionization (ESI). In all the experiments reported in this paper the analyte was a

10 μM solution of bovine Cytochrome C (Sigma Aldrich) in 50/50 water/methanol (by volume) with 0.1% formic acid to aid protonation.

The octopole is used to interface the ESI ion source and the quadrupole mass spectrometer. The ESI flow rate was maintained at 36 μL/H. The octopole has an electrode radius of 3 mm, length 170.5 mm, and an inscribed field radius of 4.5 mm. The RF potential on the octopole was maintained at $50V_{0\text{-peak}}$ and the RF frequency was set at 1 MHz. Ions with sufficient energy travel into the quadrupole mass filter, which can either operate in transmission mode (RF only mode) or mass filtering mode. There is an ion lens assembly between the octopole and the QMF, an exit electrode following the octopole, and an entrance electrode preceeding the QMF, which were all maintained at ground potential. The aperture diameter of both lens electrodes is 2 mm. Between the QMF and MCP's there is an exit electrode mounted on the QMF followed by an Einzel lens assembly which were all maintained at ground potential. The aperture diameter of the exit electrode of the QMF is ≈ 8.5 mm. The QMF has a mass range of up to 4000 *m/z*, a length of 210 mm, an electrode diameter of 9.525 mm, an inscribed field radius of 4.17 mm, and an operating frequency of 880 kHz. The RF potential on the QMF was maintained at 1000 $V_{0\text{-peak}}$.

A matched chevron MCP stack (F2225-21N290, Hamamatsu Photonics Deutschland GmbH, Herrschingam Ammersee, Germany; active area ϕ = 4 cm, 12 μm pores, 15 μm pitch) is placed in front of the Timepix chip array. Ions exiting from the quadrupole will impact on the MCPs and the resultant electron shower is projected on the Timepix chips. The dimension of an individual Timepix chip is 1.4 ×1.6 cm^2. The major characteristics of this application-specific integrated circuit (ASIC) are 256×256 pixels of 55×55 μm each per chip. In the work reported, we have employed an array of 2×2 Timepix chips. The front MCP was maintained

at -1750*V*, the back MCP at -400*V*, and the Timepix detector was at ground potential. Timepix data is acquired by the Pixelman software package.

Data and image analysis were performed using algortihms developed in Matlab-R2011b (Mathworks, Natick, USA). The QMS assembly was controlled with in house developed AWG software [17] with a fully automated data acquisition electronic drive unit for scanning of the mass filter electrode voltages.

Simulation

QMS2-Imaging

A custom trajectory simulation program (QMS2-Imaging) developed in Visual C++ environment was used. The program calculates ion trajectories by solving the Mathieu equations using a fourth order Runge-Kutta algorithm. It operates by dividing the ion trajectories into small time steps and assuming that over the steps the ion motion in three directions *x*, *y*, and *z* is uncoupled. Mass scans are computed by ramping the values of *U* and *V* with fixed *U*/*V* ratio, which sets the resolution of an instrument. The model can plot the spatial distribution of individual ions exiting the mass filter by means of tracing the exit position in the x-y plane. The final x, y (and also *m/z*) information of each ion which successfully traverses the QMF is stored.

A second routine (IonSrc) allows entry conditions for large number of ions (typically 10^8), to be specified, which are subsequently supplied to the mass filter calculation engine to simulate individual trajectories in each case. Finally, Matlab was used to post process the data and for the generation of graphical results.

Results and Discussions

Effect of ESI source operating conditions on transmission characteristics of the ion beam

Figure 2a illustrates experimentally measured effect of skimmer potential on the spatial distribution of the transmitted ion beam imparted via the octopole ion guide-quadrupole mass spectrometer (OQ) RF only beamline. The skimmer serves two main purposes when employed in the ESI source region; a) the potential on it provides the expanding ion jet with enough energy to overcome the front RF and/or DC fringe fields of the ion guide, and b) it stops the unwanted neutral molecules from entering the next higher vacuum region. For the experiments shown in Figure 2a, the capillary voltage was maintained at 120 V and the tube lens voltage was maintained at 175 V. The pressure in the octopole was maintained at 2.8E-04 mbar. It can be seen from Figure 2a that when the skimmer is supplied with a potential less than 20 V, there are no ions transmitted via the OQ beamline. A potential of 20 V on the skimmer enabled the acceleration of ions through the octopole, i.e. ions gained sufficient energy to overcome the front fringe fields to be injected into the octopole. With an increase in potential from 20 – 30 V the diameter of the ion beam increases concomitant with an increase in total ion current (TIC). Further increase in potential (30 – 100 V) has no effect on the ion beam diameter and the ion intensity remains constant. The dependence of ion intensity on skimmer potential is plotted as Figure 2b. It should also be noted that the central halo profile observed in the ion beam is a property of the supersonic jet expansion [8] between the nozzle of the capillary and the skimmer (electro hydrodynamics in the source region), and the pressure inside the source and cooling octopole region. This effect is explained further on in this paper.

Figure 2c shows dependence of ion intensity on the tube lens potential. The capillary voltage was maintained at 120 V and the skimmer voltage was maintained at 30 V for the

experiments reported in Figure 2c. The pressure in the octopole was maintained at 2.8E-04 mbar. Little fluctuation in the ion beam diameter is observed. However, an increase of capillary potential from 0-125 V increases transmission. Further increases in potential (125-300 V) decreases transmission. The increase in ion intensity can be explained by the prime role of the tube lens. Upon application of potential, the tube lens produces a declustering electric field between itself and the skimmer. The electric field breaks analyte/solvent clusters formed from the supersonic jet expansion thus increasing ion intensity. The decrease in total transmitted ion current with increase in tube lens potential beyond ~120 V cannot be explained quantitatively. However, the higher retarding field potential and the increased electrostatic force on the ions resulting in deflections at higher voltage values (which results in collision of ions at the surface of source components) determine this effect.

Collisional focusing inside RF only multipoles

In order to visualize collisional focusing inside cooling multipoles, measurements were taken at different gas pressures inside the cooling octopole region. Figure 3 shows Timepix measured spatial distributions and the total ion current of the ion beam transmitted via the OQ beamline at four different (2E-04, 2.8E-04, 3.7E-04 and 5E-04 mbar) operating pressures for the cooling octopole. From Figure 3, it clearly appears that the ion distribution imparted via the skimmer is not homogenous (it is a radially expanding distribution). The halo profile with a lower central intensity is more pronounced at lower values of gas pressure as there is less dampening of ion trajectories. With an increase in gas pressure inside the cooling multipole the transmission increases as expected as a result of increased collisional damping (collisonal focusing) of the ion trajectories, which brings ions closer to the central axis.

It should also be noted that, the central hole in the ion beam profile is expected to disappear at higher gas pressures (≥5E-04 mbar), but readings are not taken because they exceed the critical operating pressure of the micro channel. Moreover, quadrupoles are known to provide an ion beam with central maxima for a homogenous source distribution. It is the spatial distribution of the ion beam injected via octopole into quadrupole that is contributing to the final central halo profile. This effect is discussed in detail in the following section via QMS2-Imaging simulations.

Effect of initial ion beam spatial distribution on the output beam characteristics from an RF only quadrupole

The ion beam spatial distribution exiting an RF only quadrupole was simulated for two cases of ion entrance/injection conditions, a homogenous ion beam distribution and a ring shaped ion beam distribution. The simulations were performed for the case of ideal operating conditions (hyperbolic electrodes) and for m/z 894. Figure 4a shows a graphical illustration of a homogenous entrance ion beam spatial distribution into an RF only quadrupole and Figure 4b shows corresponding simulated spatial distribution of the output ion beam at the exit of the quadrupole. It should be noted that the simulation considers injection of ions at random RF phase (randomly distributed over 360 degrees of the phase angle). As seen from Figure 4b, the ion beam has a maximum intensity in the centre and the intensity decreases with increasing distance in (x, y).

Figure 4c shows a graphical illustration of an ion beam spatial distribution with a central minimum into an RF only quadrupole and Figure 4d shows the corresponding simulated spatial distribution of the output ion beam. As seen from Figure 4d, the central minimum profile has a major impact on the transmitted ion beam spatial distribution. The ring

shaped profile projects on the output ion beam spatial distribution at the exit of the quadrupole (Figure 4d). The halo gets more pronounced (Figure 4e and Figure 4f) as the ion beam traverses a certain distance (10 mm and 20mm) after the quadrupole and impacts the detector. It cannot be explicitly stated that it is only the ion entrance conditions that will contribute to a central halo profile at the output of the quadrupole in practice. Other factors such as space charge, pressure, presence of multiple charge species, beam divergence between quadrupole and detector etc. can also play a role.

Spatial distribution of ions lying within different m/z or q window exiting via an RF quadrupole

When operated in RF only mode, the QMF is operated along the q axis of the Mathieu stability diagram [18] and the QMF acts as a high-pass filter with the low mass cut off, M_{min}, given by equation 1

$$M_{min} = \frac{4eV}{0.908\omega^2 r_0^2} \quad (1)$$

Where V is the zero-to-peak amplitude of RF voltage oscillating with angular frequency ω (expressed in radians per second), e is the charge on the ion in coulombs, and r_0 is the inscribed QMS field radius. Readings were taken at different values of RF voltages in steps of 125 $V_{0\text{-}p}$ (i.e. 125 V to 1250 V) giving low mass cut off values in steps of 100 Da between 100 Da to 1000 Da respectively. To obtain a mass selected spatial distribution of ions that have as a result of the low mass cut off effect, corresponding RF readings were subtracted (e.g. 250 V – 125 V giving spatial distribution of ions lying within the window 100 Da to 200 Da) and the spatial distribution obtained is shown in Figure 5. From Figure 5 the following observations can be made:

1. The spatial distribution of ions at the exit of the quadrupole differs for each mass window(or q window). The result suggests that acceptance is different for each different mass window.
2. For ambient ionization based system and for multiple charge species, ions exit in the form of rings.
3. As the m/z increases, space charge effects are more evident; the space charge effects are more pronounced in the mass windows where different charge states of Cytochrome C lie. The higher m/z ions (800 – 900 Da and 900- 1000 Da) reveal four density maximums that face the electrode apexes. This effect is attributed to mirror-charge attraction as the positive ions induce a negative mirror charge on the surface of the QMF electrodes.
4. Addition of all the mass windows (100 – 1000 Da) gives an ion beam profile similar to the one in Figure 3 for a pressure of 5.00E-4 mbar and confirms the validity of the approach.

Investigation of factors that define the kinetic energy

The purpose of this investigation is to assess the dominant factors that define the kinetic energy of the ions exiting the cooling multipole ion guide. In the past, Katta et al [19] and Boyle et al [20] have suggested that the potential on the skimmer, pressure inside the cooling multipole ion guides and the DC bias applied to it determine the kinetic energy of the ions exiting the multipole ion guides. On the other hand Verentchikov and Ens have implied that ions of different masses gain uniform velocity in the gas jet expansion [21]. Hang and Lewis [7] have found the DC bias on the multipole ion guide to be the most dominant factor influencing the ion kinetic energy.

We have performed a retarding field analysis to check whether it is the skimmer potential or the DC bias that influences ion kinetic energy. The result (Figure 6) for our instrument (Figure 1) demonstrates that the kinetic energy of ions entering the quadrupole via a cooling octopole is dependent upon the DC bias applied to the octopole. The DC bias on the octopole was maintained at 18V and a retarding potential is applied on the exit lens of the octopole. Figure 6a shows readings taken at three different skimmer potentials (30V, 40V, and 50V) and different retarding potentials on the octopole exit lens. It is clearly observed from Figure 6a that for the three different cases, a potential of 18V on the exit lens stops ions passing through it. A similar effect is observed at a higher pressure, and it can be stated that once the ions are cooled (in a cooling multipole ion guide) then the energy of the ions entering the next region of the instrument is defined only by the DC bias applied to the octopole. A similar investigation was conducted with the exit lens potential of the quadrupole and the results are presented in Figure 6b. Surprisingly, there is reduction in ion kinetic energy by 2eV at the exit of the quadrupole compared to ion entrance kinetic energy. The complex RF and DC fringe fields at the exit of octopole, the RF fringe fields of the quadrupole and the pressure inside the quadrupole determine the extent of this effect [22].

Conclusions

Through this work using a position sensitive detector, we have provided an unparalleled experimental illustration of some well-known effects and some not so well known effects associated with ESI based mass spectrometry such as collisional focusing inside the cooling ion guide, space charge in the ion guides. The Timepix position sensitive detector was used to systematically investigate, visualize and directly measure the fine details of the ion beam intensity distribution under various operating conditions for the ion guides. The effect of skimmer and tube lens potential on the ion beam spatial distribution and transmission

characteristics were studied. The ion beam diameter and transmission were found to increase at lower values of skimmer potential (20V to 30V) and with further increase in potential (30V to 40V) they remain constant. Moreover, we have experimentally shown the effect of collisional focusing inside cooling multipole ion guide on the spatial distribution of the ion beam. This demonstrated how collisional cooling brings ions closer to central axis and increases transmission efficiency accordingly.

Experimental results also suggest that the spatial distribution of the ion beam exiting the RF only quadrupole is heavily influenced by the spatial distribution of the ion beam injected. Our experimental findings were confirmed with in-silico simulations. Ion distributions at various mass windows of a cytochrome C ion beam that contains various multiply charged species were analyzed experimentally using the Timepix detector. The spatial distribution at different mass windows is different compared to each other, with heavy *m/z* ions more prone to space charge effects. We have also performed retarding field analysis at the collisional cooling multipole ion guide in order to determine which potential or ion optical element really defines the kinetic energy of the ion beam. The DC bias applied to the collisional cooling multipole ion guide is found to be the most dominant factor that determines the ions kinetic energy in this system.

Figure Legends

Figure 1: 2D schematic presentation with visualization of absolute potential distribution of the system.

Figure 2: a) Timepix measured spatial distribution of the OQ beamline at different operating potentials of the skimmer; b) Dependence of ion intensity on skimmer potential; c) Dependence of ion intensity on the tube lens potential.

Figure 3: Experimentally measured effect of the pressure inside the cooling octopole on transmitted ion beam distributions through a RF only quadrupole, (top) spatial distribution of the ion beam, (bottom) total hits recorded on the Timepix.

Figure 4: a) Graphical illustration of a uniform source distribution; b) Simulated output ion beam spatial distribution from an RF only quadrupole for an injected ion beam illustrated in (a); c) Graphical illustration of a central halo source distribution; d) Simulated output ion beam spatial distribution from an RF only quadrupole for an injected ion beam illustrated in (c); e) Simulated output ion beam spatial distribution from an RF only quadrupole for an ion beam illustrated in (c) and as it traverses a distance of 10 mm at the exit side. f) Simulated output ion beam spatial distribution from an RF only quadrupole for an ion beam illustrated in (c) and as it traverses a distance of 20 mm at the exit side.

Figure 5: Spatial distribution of ions of Cytochrome C protein complex lying in different mass windows (or q windows) from an RF only quadrupole

Figure 6: a) Variation of ion intensity as a function of octopole exit lens potential; b) Variation of ion intensity as a function of quadrupole exit lens potential

Acknowledgments

This research received funding from the Netherlands Organisation for Scientific Research (NWO) in the framework of the Technology Area COAST. This work is part of the research program of the Foundation for Fundamental Research on Matter (FOM), which is part of the Netherlands Organization for Scientific Research (NWO). The authors acknowledge Ronald Buijs, Marc Duursma, and Frans Giskes of AMOLF for their contribution to the experiments.

References

1. Dawson, P. H., French, J. B., Buckley, J. A., Douglas, D. J., & Simmons, D. (1982). The use of triple quadrupoles for sequential mass spectrometry: 1—The instrument parameters. *Organic Mass Spectrometry*, *17*(5), 205-211.
2. Bier, M. E., & Syka, J. E. (1995). *U.S. Patent No. 5,420,425*. Washington, DC: U.S. Patent and Trademark Office.
3. André, J. (1976). Étude théorique de l'influence des collisions élastiques sur un gaz dilué de particules chargées, confinées par un champ de radio-fréquence à symétrie quadrupolaire. *Journal de Physique*, *37*(6), 719-730.
4. Bonner, R. F., March, R. E., & Durup, J. (1976). Effect of charge exchange reactions on the motion of ions in three-dimensional quadrupole electric fields.*International Journal of Mass Spectrometry and Ion Physics*, *22*(1), 17-34.
5. Bonner, R. F., & March, R. E. (1977). The effects of charge exchange collisions on the motion of ions in three-dimensional quadrupole electric fields Part II. Program improvements and fundamental results. *International Journal of Mass Spectrometry and Ion Physics*, *25*(4), 411-431.
6. Douglas, D. J., & French, J. B. (1992). Collisional focusing effects in radio frequency quadrupoles. *Journal of the American Society for Mass Spectrometry*, *3*(4), 398-408.
7. Hang, W., Lewis, C., & Majidi, V. (2003). Practical considerations when using radio frequency-only quadrupole ion guide for atmospheric pressure ionization sources with time-of-flight mass spectrometry. *Analyst*, *128*(3), 273-280.
8. Chernushevich, I. V., & Thomson, B. A. (2004). Collisional cooling of large ions in electrospray mass spectrometry. *Analytical chemistry*, *76*(6), 1754-1760.

9. Tolmachev, A. V., Udseth, H. R., & Smith, R. D. (2000). Charge capacity limitations of radio frequency ion guides in their use for improved ion accumulation and trapping in mass spectrometry. *Analytical chemistry*, *72*(5), 970-978.
10. Tolmachev, A. V., Udseth, H. R., & Smith, R. D. (2000). Radial stratification of ions as a function of mass to charge ratio in collisional cooling radio frequency multipoles used as ion guides or ion traps. *Rapid Communications in Mass Spectrometry*, *14*(20), 1907-1913.
11. Tolmachev, A. V., Udseth, H. R., & Smith, R. D. (2003). Modeling the ion density distribution in collisional cooling RF multipole ion guides. *International Journal of Mass Spectrometry*, *222*(1), 155-174.
12. Tolmachev, A., Harkewicz, R., Alving, K., Masselon, C., Anderson, G., Rakov, V., Pasa-Tolic, L., Nikolaev, E., Belov, M., Udseth, H., & Smith, R.D. (2000). Radial stratification of ions as a function of m/z ratio in collisional cooling rf multipoles used as ion guides or ion traps. *Proceedings of the 48th ASMS Conference*, Long Beach, CA, June 11–15, p. 115 (CD ROM)
13. Syed, S. U., Eijkel, G. B., Kistemaker, P., Ellis, S., Maher, S., Smith, D. F., & Heeren, R. M. (2014). Experimental investigation of the 2D ion beam profile generated by an ESI Octopole-QMS system. *Journal of The American Society for Mass Spectrometry*, *25*(10), 1780-1787.
14. Syed, S. U., Eijkel, G. B., Maher, S., Kistemaker, P., Taylor, S., & Heeren, R. M. (2014). A micropixelated ion-imaging detector for mass resolution enhancement of a QMS instrument. *Analytical and bioanalytical chemistry*, 1-8.
15. Jungmann, J. H., Smith, D. F., MacAleese, L., Klinkert, I., Visser, J., & Heeren, R. M. (2012). Biological tissue imaging with a position and time sensitive pixelated detector. *Journal of the American Society for Mass Spectrometry*,*23*(10), 1679-1688.
16. Jungmann, J. H., Smith, D. F., Kiss, A., MacAleese, L., Buijs, R., & Heeren, R. (2013). An in-vacuum, pixelated detection system for mass spectrometric analysis and imaging of macromolecules. *International Journal of Mass Spectrometry*, *341*, 34-44.
17. Taban, I. M., van der Burgt, Y. E., Duursma, M., Takats, Z., Seynen, M., Konijnenburg, M., ... & Heeren, R. (2008). A novel workflow control system for Fourier transform ion cyclotron resonance mass spectrometry allows for unique on-the-fly data-dependent decisions. *Rapid Communications in Mass Spectrometry*, *22*(8), 1245-1256.
18. Dawson, P. H. (1976). Quadrupole mass spectrometry and its applications.

19. Katta, V., Chowdhury, S. K., & Chait, B. T. (1991). Use of a single-quadrupole mass spectrometer for collision-induced dissociation studies of multiply charged peptide ions produced by electrospray ionization. *Analytical chemistry*, *63*(2), 174-178.
20. Boyle, J. G., & Whitehouse, C. M. (2002). Time-of-flight mass spectrometry with an electrospray ion beam. *Analytical chemistry*, *64*(18), 2084-2089.
21. Verentchikov, A. N., Ens, W., & Standing, K. G. (1994). Reflecting time-of-flight mass spectrometer with an electrospray ion source and orthogonal extraction.*Analytical chemistry*, *66*(1), 126-133.
22. Gibson, J. R., Evans, K. G., Syed, S. U., Maher, S., & Taylor, S. (2012). A method of computing accurate 3D fields of a quadrupole mass filter and their use for prediction of filter behavior. *Journal of the American Society for Mass Spectrometry*, *23*(9), 1593-1601.

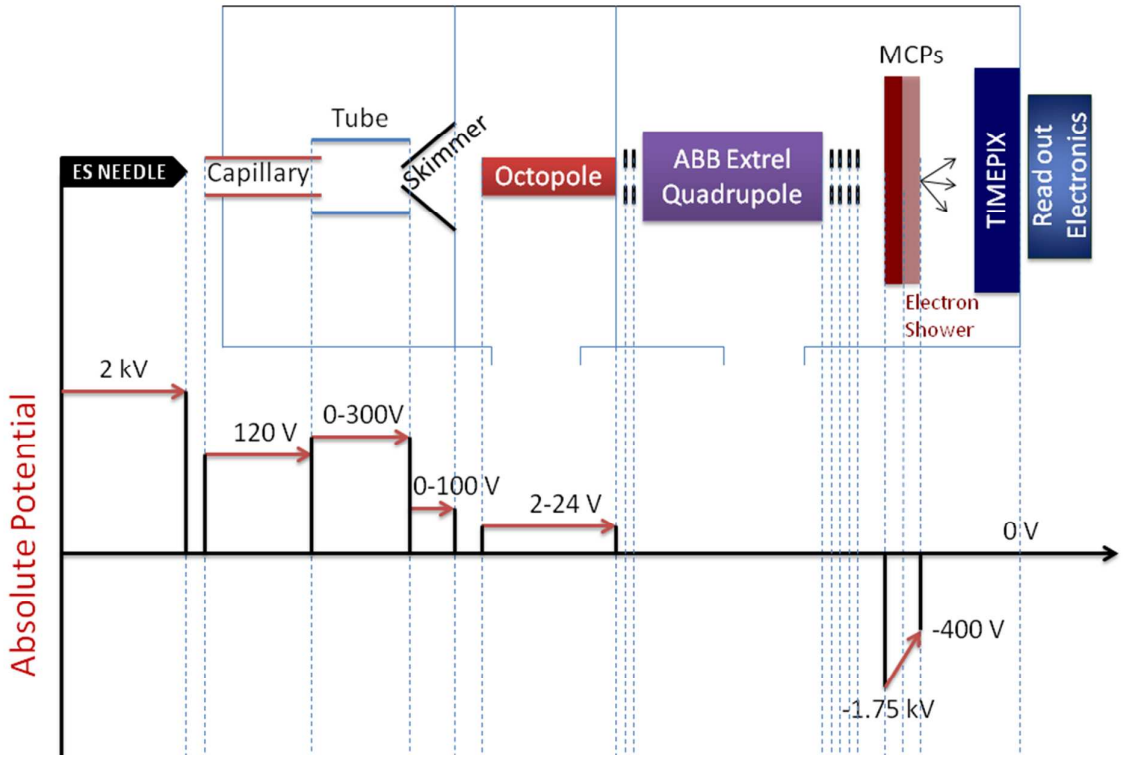

Figure 1: 2D schematic presentation with visualization of absolute potential distribution of the system.

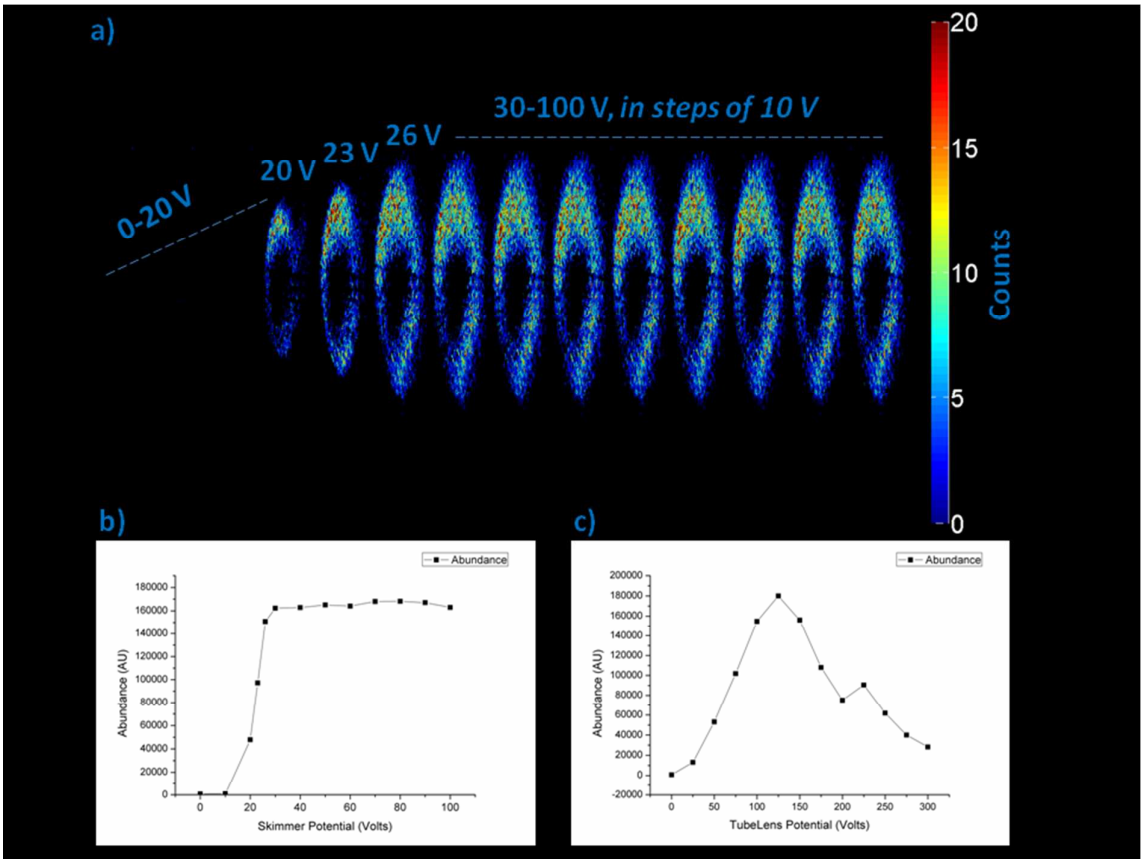

Figure 2: a) Timepix measured spatial distribution of the OQ beamline at different operating potentials of the skimmer; b) Dependence of ion intensity on skimmer potential; c) Dependence of ion intensity on the tube lens potential.

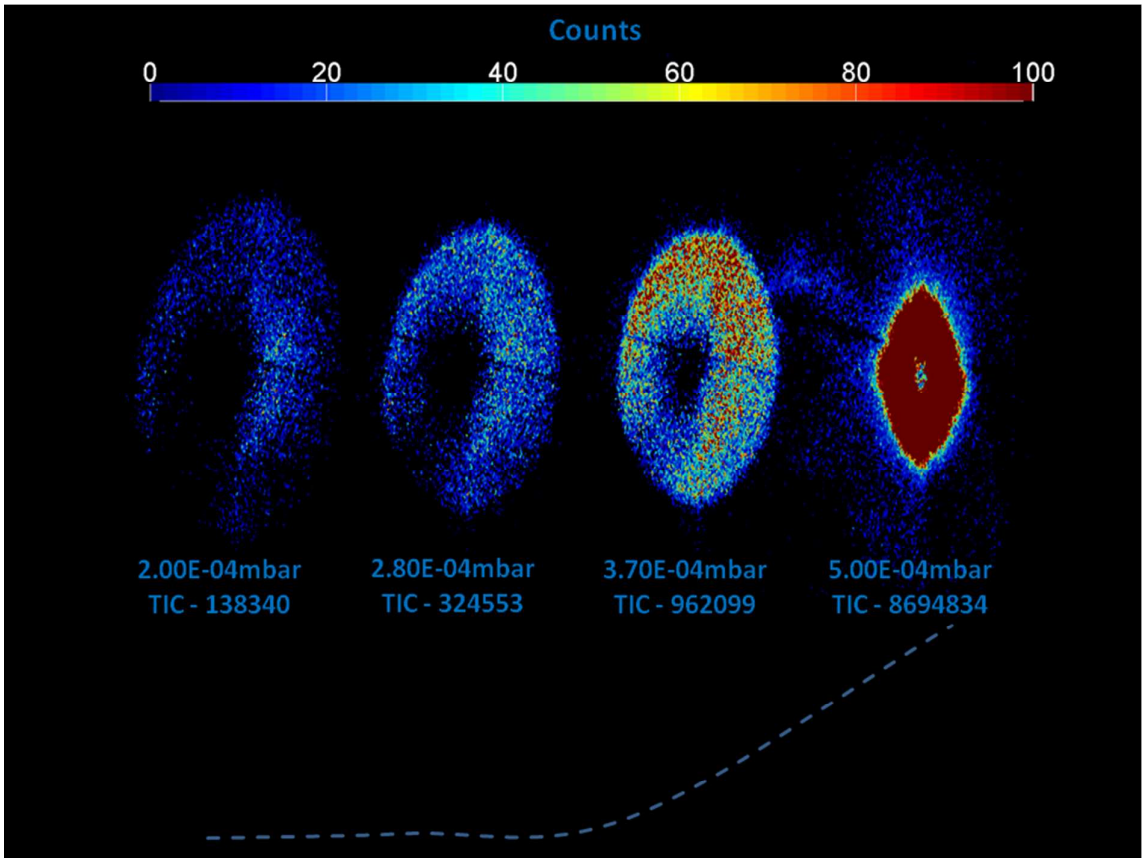

Figure 3: Experimentally measured effect of the pressure inside the cooling octopole on transmitted ion beam distributions through a RF only quadrupole, (top) spatial distribution of the ion beam, (bottom) total hits recorded on the Timepix.

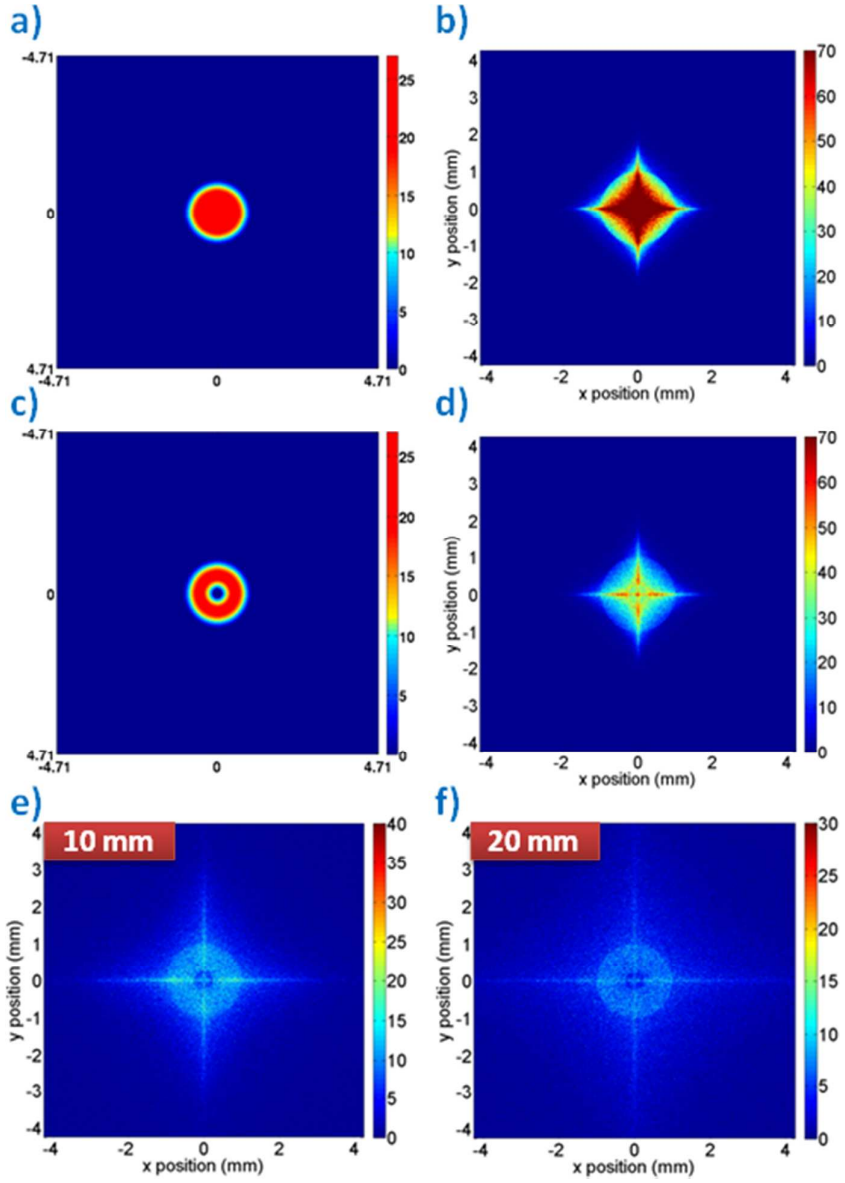

Figure 4: a) Graphical illustration of a uniform source distribution; b) Simulated output ion beam spatial distribution from an RF only quadrupole for an injected ion beam illustrated in (a); c) Graphical illustration of a central halo source distribution; d) Simulated output ion beam spatial distribution from an RF only quadrupole for an injected ion beam illustrated in (c); f) Simulated output ion beam spatial distribution from an RF only quadrupole for an ion beam illustrated in (c) and as it traverses a distance of 10 mm at the exit side. e) Simulated output ion beam spatial distribution from an RF only quadrupole for an ion beam illustrated in (c) and as it traverses a distance of 20 mm at the exit side.

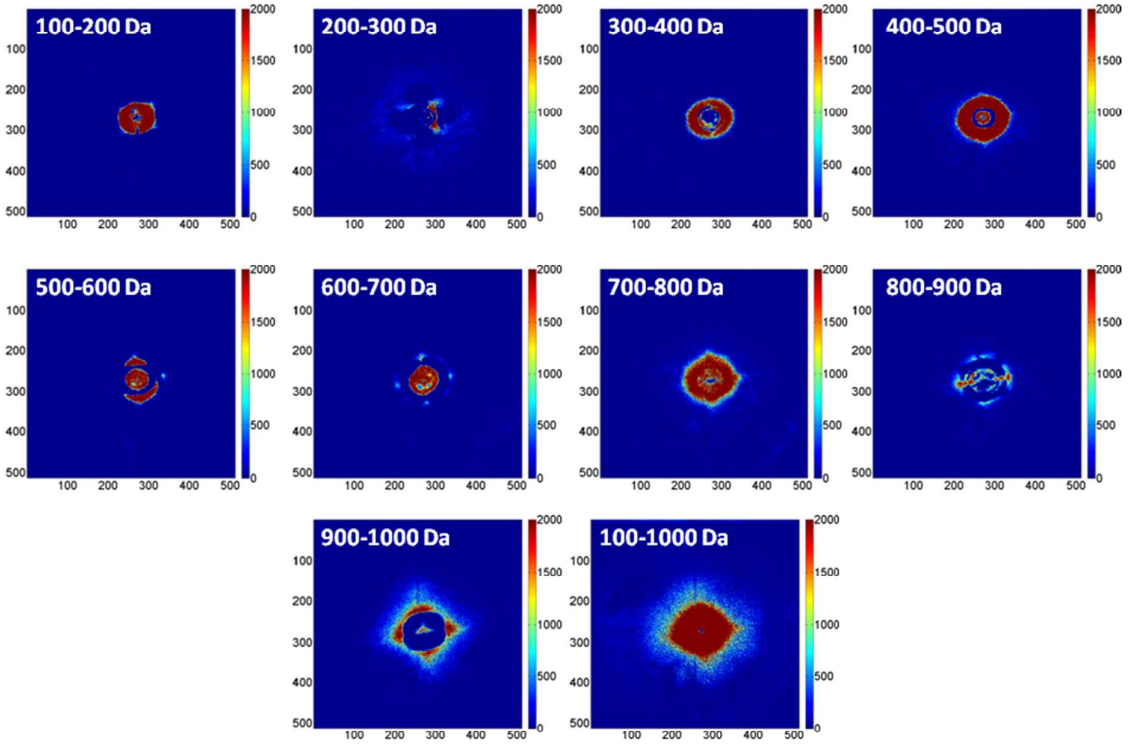

Figure 5: Spatial distribution of ions of Cytochrome C protein complex lying in different mass windows (or q windows) from an RF only quadrupole

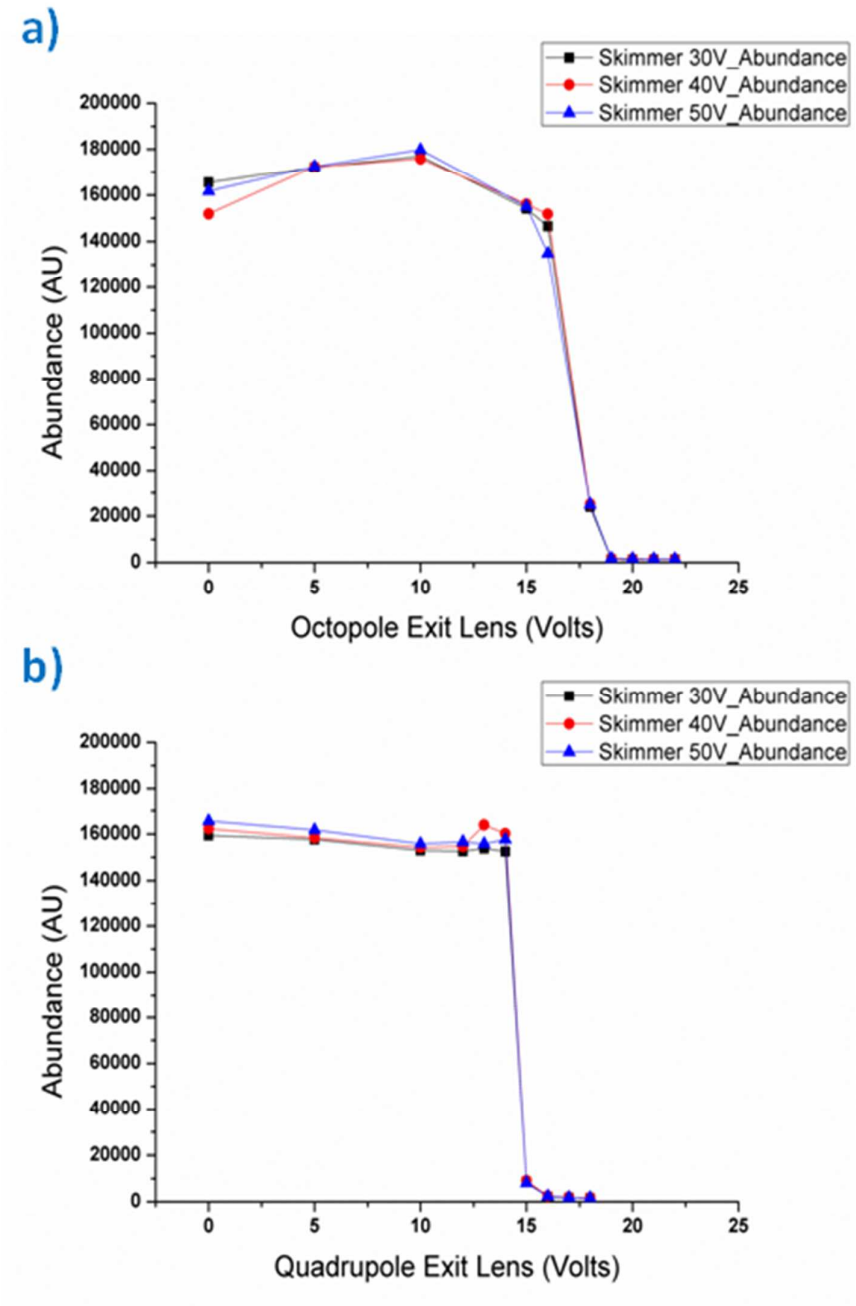

Figure 6: a) Variation of ion intensity as a function of octopole exit lens potential; b) Variation of ion intensity as a function of quadrupole exit lens potential